Iron Loss Analysis of Permanent-Magnet Machines by Considering Hysteresis Loops Affected by Multi-Axial Stress

Katsumi Yamazaki[1], Yoshito Sato[1], Mathieu Domenjoud[2], and Laurent Daniel[2]

[1]Chiba Institute of Technology, Narashino 275-0016, Japan
[2]GeePs–Group of Electrical Engineering-Paris, UMR CNRS 8507, CentraleSupélec, University of Paris-Sud, Université Paris-Saclay, Sorbonne Université, 91192 Gif-sur-Yvette, France

This article describes a method to calculate iron loss of permanent-magnet machines by considering the hysteresis loops affected by multi-axial stress. A simple hysteresis model is introduced and modified by reluctivity and hysteresis loss increase ratios, which can be determined by core material experiments under uniaxial stress. This model is coupled with time-stepping finite-element analysis. The validity of the proposed method is confirmed by the core material experiments under multi-axial stress and measured characteristics of permanent-magnet machines. It is clarified that the accuracy of the proposed method is acceptable.

Index Terms— Finite-element methods, losses, permanent-magnet machines, stress.

I. INTRODUCTION

THERE are many articles that reported an increase in iron loss of permanent-magnet machines by mechanical stress caused by shrink fitting and centrifugal force. The increase in the iron loss must have been mainly caused by the variation in hysteresis loops with stress. However, in most of the articles, the effects of stress were taken into account in anhysteretic electromagnetic-field calculation only by modifying the reluctivity and core loss using the increase ratios due to stress [1]–[3]. Bernard and Daniel [4] expanded the Jiles–Atherton hysteresis model to estimate the variation in hysteresis loops. Kai *et al.* [5] reported a model of vector magnetic property that takes stress into account. However, there is no article, in which the measured motor characteristics are compared with the calculated results considering hysteresis loops affected by multiaxial stress. It is considered that a simpler and straightforward method is desired, particularly for the calculation of cogging torque because the accurate and stable solution of the magnetic field is required.

From these viewpoints, in this article, we introduce a simple hysteresis model for direct consideration of the effects of multi-axial stress in the governing equation of finite-element analysis (FEA). The parameters required for this model can be determined by core material experiments under uniaxial stress. The validity of the proposed method is confirmed by core material experiments under multi-axial loading configuration and measured characteristics of permanent-magnet machines.

II. CALCULATION METHOD

A. Previous Method for Stress and Hysteresis Loss

In [3], the increase ratios of reluctivity ν and hysteresis loss w_h of the core material due to mechanical stress are introduced

in the anhysteretic FEA, as follows:

$$\nu'(\sigma_{\text{eq}}, B) = C_\nu(\sigma_{\text{eq}}, B)\nu(B) \tag{1}$$

$$w_h'(\sigma_{\text{eq}}, B_m) = C_h(\sigma_{\text{eq}}, B_m)w_h(B_m) \tag{2}$$

where C_ν, C_h, ν', and w_h' are the increase ratios and modified values of ν and w_h due to stress, B is the absolute value of flux density vector, B_m is the amplitude of B, and σ_{eq} is the equivalent stress, which can be expressed as follows:

$$\sigma_{\text{eq}} = \frac{3}{2}\,\vec{h}\,s\,\vec{h} \tag{3}$$

where $\vec{h}$ is the unit vector along the magnetic-field direction, s is the deviatoric part of the stress tensor expressed from the multi-axial stress imposed on the core. By using σ_{eq}, C_ν and C_h can be determined from experiments on the core material under uniaxial stress imposed along the flux direction. In [3], the increase ratio of hysteresis loss C_h is used only for the correction factor of hysteresis loss, which is obtained by post calculation of the anhysteretic FEA.

B. Proposed Method With Hysteresis Modeling

In [6], a simple hysteresis modeling shown in Fig. 1 is proposed. In this model, the magnetic field on the major hysteresis loop H_{major} is expressed by three terms, as follows:

$$H_{\text{major}}(B_m, B) = \nu(B)B + H_s(B_m, B) + H_w(B_m, B). \tag{4}$$

The first term corresponds to the B–H curve used in the anhysteretic FEA. This curve can be obtained by the average curve of the largest major hysteresis loop in experiments on the core material. On the other hand, H_s and H_w are the shift value of the average hysteresis curve and the width of the hysteresis loop, respectively.

By considering (1), (2), (4), in this article, the major hysteresis loop affected by the multi-axial stress H_{major}' is expressed, as follows:

$$\begin{aligned}
H_{\text{major}}'&(B_m, B)\\
&= C_\nu(\sigma_{\text{eq}}, B)\nu(B)B\\
&\quad + C_h(\sigma_{\text{eq}}, B_m)\{H_s(B_m, B) + H_w(B_m, B)\}. \tag{5}
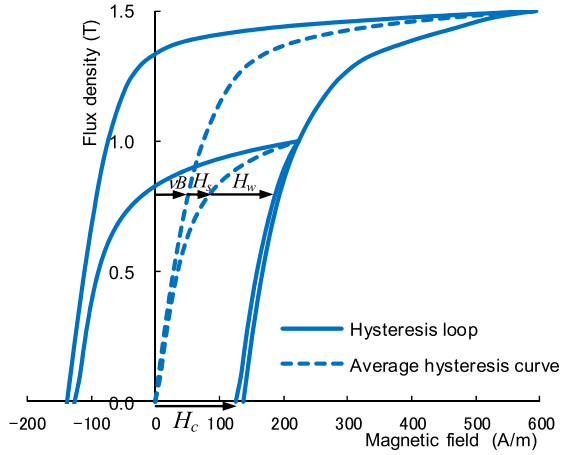\end{aligned}$$

Fig. 1.   Simple modeling of the hysteresis loop.

TABLE I
PARAMETERS FOR HYSTERESIS LOSS INCREASE RATIO DUE TO STRESS

Type of steel sheet	$C_{h,\max}$	B_h	σ_h
Low grade	4.9	0.7	100
High grade	5.5	0.7	100

In this model, ν is modified by C_ν, whereas H_s and H_w are modified by C_h. These modifications can be applied when the hysteresis loop is expressed by the three terms as in (4).

C. Determination of Model Parameters

For the stability of FEA, the reluctance and hysteresis loss increase ratios C_ν and C_h are approximated by simple functions of flux density B and equivalent stress σ_{eq} from the material experiments as follows [7]:

$$C_\nu(\sigma_{eq}, B) = K_d(B)\sigma_{eq} + 1 \tag{6}$$

$$C_h(\sigma_{eq}, B) = 1 + \left\{ (C_{h,\max} - 1) \exp\left(-\frac{B}{B_h}\right) \right\}$$
$$\times \left\{ 1 - \exp\left(\frac{\sigma_{eq}}{\sigma_h}\right) \right\} \tag{7}$$

where K_d, $C_{h,\max}$, B_h, and σ_h are the model parameters that are adjusted to experiments on the core material under uniaxial stress imposed along the flux direction. The detailed method for this parameter determination is reported in [7].

Figs. 2 and 3 show the measured reluctivity and loss increase ratios of an electrical steel sheet. In the measurement, the results of two rectangular samples, whose longitudinal directions are adjusted to rolling and transverse directions, are averaged. The approximated values by (6) and (7) are also shown. The figures indicate that both reluctivity and loss considerably increase with compressive stress (negative stress), whereas the variations with the tensile stress (positive stress) are very small. Therefore, the parameters in (6) and (7) are adjusted by using the measured results under compressive stress. On the other hand, both C_ν and C_h for tensile stress are approximated to be 1.0.

Table I lists the adjusted parameters in the cases of low grade (little silicon) and high-grade steels (3% silicon). $C_{h,\max}$ for the high-grade steel is determined to be larger than that
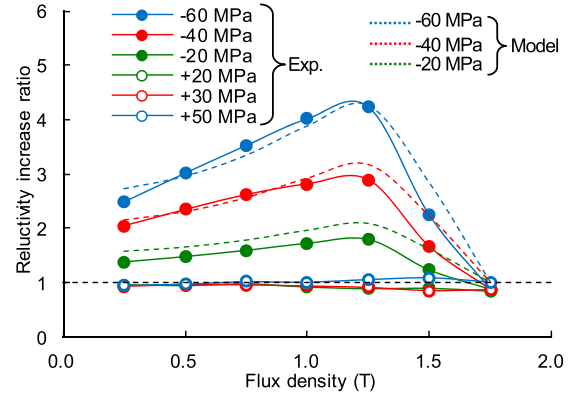

Fig. 2.   Measured and modeled reluctivity increase ratios (low-grade steel).
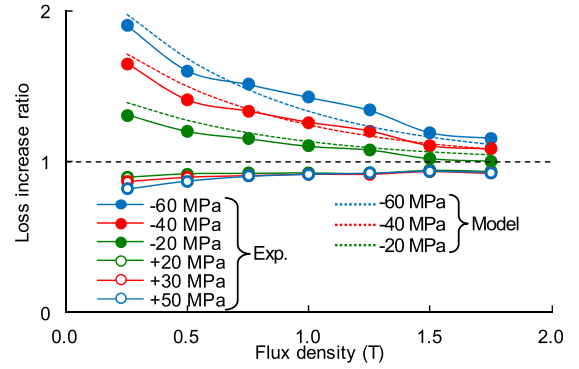

Fig. 3.   Measured and modeled loss increase ratios (low-grade steel).

of the low-grade one. It implies that the effect of stress on hysteresis loss is larger in high-grade steel.

H_s and H_w in the hysteresis model are also approximated by the combination of power and exponential functions, as follows [6]:

$$H_w(B_m, B)$$
$$= H_c(B_m) \left\{ 1 - \left(\frac{B}{B_m}\right)^{a_w + b_w B_m} \right\}$$
$$+ C_w(B_m)[\exp\{-\beta_w(B_m - B)\}$$
$$- \exp\{-\gamma_w(B_m)(B_m - B)\}] \tag{8}$$

$$H_s(B_m, B)$$
$$= H_w(B_{\max}, B) \left\{ 1 - \exp\left(-\frac{B}{B_s}\right) \right\} \left(\frac{B}{B_m}\right)^{a_s + b_s B}$$
$$- C_s(B_m)[\exp\{-\beta_s(B_m - B)\} - \exp\{-\gamma_s(B_m)(B_m - B)\}] \tag{9}$$

where H_c is the coercive force; $B_{\max}$ is the peak-flux density of the loop whose average curve is used for $\nu(B)$ in (4); and a_w, b_w, β_w, γ_w, C_w, a_s, b_s, β_s, B_s, γ_s, and C_s are the model parameters that are adjusted to measured hysteresis loops. The minor hysteresis loops can also be approximately calculated by the combination of the major loops using (8) and (9).

Table II lists the adjusted parameters in (8) and (9). β_w for the high-grade steel is determined to be larger than that of the low-grade one. By using these parameters and B, the hysteresis loop can be calculated within negligible computational time compared with the computational time of the matrix solver.

TABLE II
PARAMETERS FOR HYSTERESIS LOOP MODELING

Type of steel sheet	a_w	b_w	β_w	a_s	b_s	β_s	B_s
Low grade	2.1	4.8	4.4	1.0	6.1	4.5	0.15
High grade	2.1	4.8	6.5	1.0	6.1	4.5	0.15

III. RESULTS AND DISCUSSION

A. Verification by Material Experiments

First, the validity of the proposed modeling for the effects of the stress on the hysteresis loop is verified by the core material experiments under multi-axial stress [8]. The specimen is the high-grade electrical steel sheet with 3% silicon. The frequency is set to be 50 Hz. The magnetic field H is measured by a calibrated H-coil placed at the surface of the specimen, whereas the flux density B is measured by using a needle-B sensor. The multiaxial stress is controlled by two actuators [8].

The following three cases are more specifically examined

1) without stress;
2) with compressive 100 MPa stress along the flux direction;
3) with tensile 100 MPa stress perpendicular to the flux.

The measured results include the reaction magnetic field of eddy currents. Therefore, in the calculation, both eddy currents and hysteresis phenomenon are estimated by 1-D FEA along the thickness of the sheet with the proposed modeling. In this case, the governing equation is expressed as follows:

$$\frac{\partial}{\partial z}\left(\nu_{1D}\frac{\partial A_{1D}}{\partial z}\right) = \frac{1}{\rho}\frac{\partial A_{1D}}{\partial t} + \frac{\partial H_{\text{hys},1D}}{\partial z}. \quad (10)$$

z is the thickness direction of the steel sheet, A_{1D} is the magnetic vector potential in the 1-D FEA, ρ is the electrical resistivity, and ν_{1D} and $H_{\text{hys},1D}$ are the reluctivity and reaction field due to the hysteresis phenomenon considering the stress, respectively, which are expressed according to the proposed modeling (5), as follows:

$$\nu_{1D} = C_\nu(\sigma_{\text{eq}}, B)\nu(B) \quad (11)$$
$$H_{\text{hys},1D} = -C_h(\sigma_{\text{eq}}, B_m)\{H_s(B_m, B) + H_w(B_m, B)\}. \quad (12)$$

The average flux density along the thickness is adjusted to the experiment by using boundary condition at the surface of the sheet. This 1-D FEA is iteratively carried out to determine $H_{\text{hys},1D}$ by using the under-relaxation method [6].

Fig. 4 shows the measured and calculated hysteresis loops. It is observed that the calculated results well express the effect of multiaxial loading configuration even though only the measured results under the uniaxial stress along the flux direction are used.

B. Applications to Permanent-Magnet Machines

Next, the proposed modeling is applied to the combined stress-electromagnetic FEAs of permanent-magnet machines.

Fig. 5 shows the cross section of the machine manufactured by the IEE-Japan rotating machine committee [9]. The stator diameter is 136 mm. The used electrical steel sheet is the low-grade one. An aluminum housing is fit to this stator core. The displacement of the stator surface by the shrink-fitting stress is designed to be 10 μm, which is used for the boundary condition of the stress analysis [3]. The core is manufactured
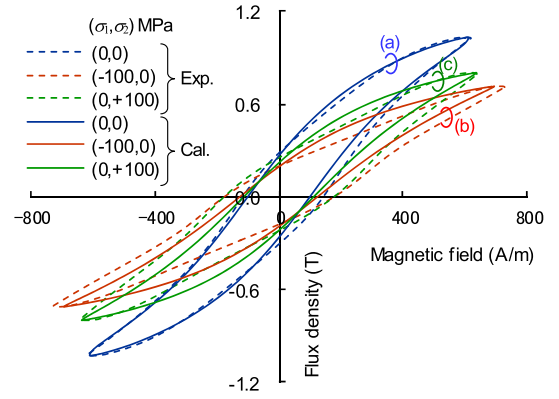

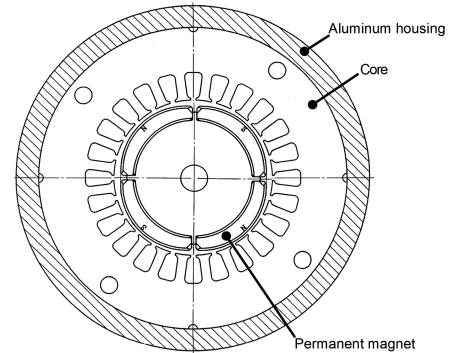Fig. 4. Measured and calculated hysteresis loops of the core material.

Fig. 5. Analyzed permanent-magnet machine.

by using wire-cutting technique to decrease the deterioration of core characteristics except for the shrink fitting. The same stator core without the housing is also manufactured.

To measure the iron loss under no-load conditions, these machines are driven by another motor, and the torque τ is measured by a torque meter. Then, the experimental no-load iron loss is obtained as follows:

$$W_i = \tau\omega_m - W_m \quad (13)$$

where ω_m is the angular speed of the rotor and W_m is the mechanical loss, which is also obtained by the measured torque before the magnetization of permanent magnets.

The electromagnetic-field analysis is carried out by the coupled 2-D-1-D FEAs [6] with an approximation of two-axis decomposition of the rotational magnetic field. The governing equation of the 2-D FEA in the core region is as follows:

$$\nabla \times (\nu_{2D}\nabla \times \boldsymbol{A}_{2D}) = \nabla \times \boldsymbol{H}_{\text{eddy,ave}} + \nabla \times \boldsymbol{H}_{\text{hys,ave}} \quad (14)$$

where ν_{2D} is the reluctivity whose expression is identical to ν_{1D} in (11); $\boldsymbol{A}_{2D}$ is the magnetic vector potential in the 2-D FEA; and $\boldsymbol{H}_{\text{eddy,ave}}$ and $\boldsymbol{H}_{\text{hys,ave}}$ are the reaction fields caused by eddy currents and the hysteresis phenomenon, respectively. They are obtained by averaging the results of the coupled 1-D FEA along the thickness of the electrical steel sheet.

Fig. 6 shows the locus of the flux-density vector at each point of the stator, in which the L-axis is defined to be the direction of $\boldsymbol{B}_{2D}$ when $|\boldsymbol{B}_{2D}|$ becomes maximum and the S-axis is orthogonal to the L-axis. The flux-density vector $\boldsymbol{B}_{2D}$ obtained by the 2-D FEA in each finite element is decomposed into the components of these axes B_L and B_S and given to the 1-D FEA the same way as in Section III-A, in order to
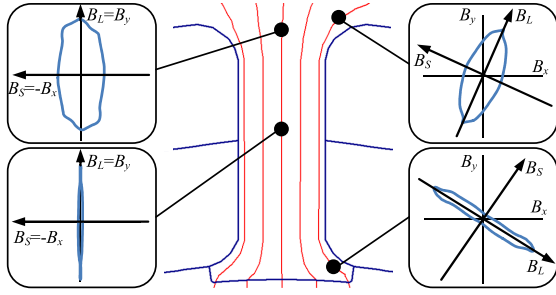
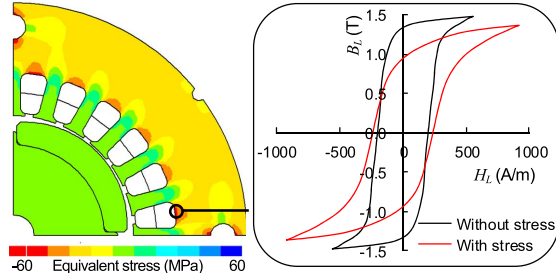Fig. 6.   Locus of flux-density vector and decomposition in 2-D FEA.

Fig. 7.   Calculated equivalent stress distribution and hysteresis loop.

calculate S- and L-axis components of the magnetic vector potential. Then, the proposed model (5) is applied to the L and S components of flux density $B_{1D,L}$ and $B_{1D,S}$ obtained by the 1-D FEA, respectively, to obtain the L and S components of magnetic field $H_{1D,L}$ and $H_{1D,S}$. Finally, the reaction field of the hysteresis phenomenon $\boldsymbol{H}_{\text{hys,ave}}$ is calculated as follows:

$$\boldsymbol{H}_{\text{hys,ave}} = \boldsymbol{R}\frac{2}{h}\int_0^{h/2}(\nu_{2D}\boldsymbol{B}_{2D} - \boldsymbol{H}_{1D})dz \tag{15}$$

where $\boldsymbol{B}_{2D} = (B_L, B_S)$, $\boldsymbol{H}_{1D} = (H_{1D,L}, H_{1D,S})$, h is the thickness of the steel sheet, and $\boldsymbol{R}$ is the rotation matrix to reset the coordinate from the LS axes to xy axes.

These 2-D and 1-D FEAs are iteratively carried out to determine the reaction field using an under-relaxation method [6]. Then, the hysteresis loss per volume is calculated from the solution of 1-D FEA as follows:

$$w_h = \frac{2}{h}\int_0^{h/2}\frac{1}{T}\oint \boldsymbol{H}_{1D} \cdot d\boldsymbol{B}_{1D}dz \tag{16}$$

where T is the time period. In this expression, the vector magnetic property is neglected and the total core loss is assumed to be the sum of the losses caused by B_L and B_S, separately. The eddy current loss and $\boldsymbol{H}_{\text{eddy,ave}}$ are also calculated from the eddy currents obtained by the 1-D FEA.

Fig. 7 shows the distribution of σ_{eq} due to the displacement of the stator core by the shrink fitting and the hysteresis loops with/without the stress. The largest compressive stress is generated at the slot bottom, where the hysteresis loop is considerably changed by stress.

Table III lists the measured and calculated no-load iron losses. The result obtained by the anhysteretic conventional method [3] is also shown. The calculation errors of both the proposed and conventional methods are around 5%. The loss underestimation must have been caused by the neglect of in-plane eddy currents. On the other hand, Fig. 8 shows the calculated cogging torque waveforms. The average value

TABLE III
MEASURED AND CALCULATED NO-LOAD IRON LOSSES (W)

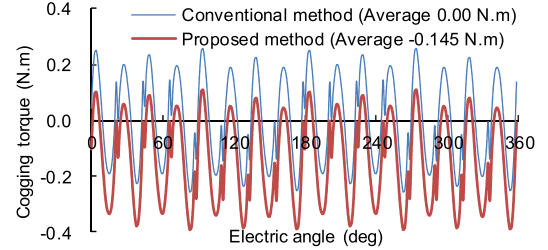|	Without stress			With stress		
	Con.	Pro.	Exp.	Con.	Pro.	Exp.
Core hysteresis loss	14.47	13.96	-	16.13	15.72	-
Core eddy current loss	7.00	7.10	-	7.00	7.01	-
Magnet eddy current loss	0.16	0.16	-	0.16	0.16	-
total	21.64	21.22	21.65	23.29	22.89	24.28

Fig. 8.   Calculated cogging torque waveforms with stress.

obtained by the conventional method is zero, whereas that by the proposed method is -0.145 N · m, which agrees well with the measured torque excluding the mechanical-loss effect (0.154 N · m). The calculation error is 6% in this case.

IV. CONCLUSION

A simple model for estimating the effects of multi-axial stress on hysteresis loop of electrical steel sheets is proposed. The validity of the model is confirmed by the experiments of core material and application to permanent-magnet machines. The results of the FEA employing the proposed model are also compared with those by conventional FEA, in which the hysteresis loss is calculated by postprocedure with stress-correction factor. It is clarified that the accuracies of the iron loss are nearly identical to each other, whereas the accuracy of the torque is significantly improved by the proposed method.

REFERENCES

[1] A. Daikoku *et al.*, "An accurate magnetic field analysis for estimating motor characteristics taking account of stress distribution in the magnetic core," *IEEE Trans. Ind. Appl.*, vol. 42, no. 3, pp. 668–674, May/Jun. 2006.

[2] M. Nakano *et al.*, "High-precision calculation of iron loss by considering stress distribution of magnetic core," *IEEJ Trans. Ind. Appl.*, vol. 129, no. 11, pp. 1060–1067, 2009.

[3] K. Yamazaki, H. Mukaiyama, and L. Daniel, "Effects of multi-axial mechanical stress on loss characteristics of electrical steel sheets and interior permanent magnet machines," *IEEE Trans. Magn.*, vol. 54, no. 3, Mar. 2018, Art. no. 1300304.

[4] L. Bernard and L. Daniel, "Effect of stress on magnetic hysteresis losses in a switched reluctance motor: Application to stator and rotor shrink fitting," *IEEE Trans. Magn.*, vol. 51, no. 9, Sep. 2015, Art. no. 7002513.

[5] Y. Kai, Y. Tsuchida, and M. Enokizono, "Vector magnetic characteristic analysis of a permanent magnet motor by controlling local stress," *IEEE Trans. Magn.*, vol. 51, no. 3, Mar. 2015, Art. no. 8101904.

[6] K. Yamazaki and Y. Takaki, "Iron loss analysis of permanent magnet motors by considering minor hysteresis loops caused by inverters," *IEEE Trans. Magn.*, vol. 55, no. 6, Jun. 2019, Art. no. 1300304.

[7] K. Yamazaki and H. Takeuchi, "Impact of mechanical stress on characteristics of interior permanent magnet synchronous motors," *IEEE Trans. Ind. Appl.*, vol. 53, no. 2, pp. 963–970, Mar./Apr. 2017.

[8] M. Rekik, O. Hubert, and L. Daniel, "Influence of a multiaxial stress on the reversible and irreversible magnetic behaviour of a 3%Si-Fe alloy," *Int. J. Appl. Electromagn. Mech.*, vol. 44, no. 3, pp. 301–315, 2014.

[9] H. Domeki *et al.*, "Investigation of benchmark model for estimating iron loss in rotating machine," *IEEE Trans. Magn.*, vol. 40, no. 2, pp. 794–797, Mar. 2004.